Universiteit
Leiden
The Netherlands

The sky is made of lava: how lava worlds reveal their interiors through their atmospheres

Buchem, C.P.A. van

Citation

Buchem, C. P. A. van. (2025, September 5). *The sky is made of lava: how lava worlds reveal their interiors through their atmospheres*. Retrieved from https://hdl.handle.net/1887/4259796

Version:	Publisher's Version
License:	Licence agreement concerning inclusion of doctoral thesis in the Institutional Repository of the University of Leiden
Downloaded from:	https://hdl.handle.net/1887/4259796

Note: To cite this publication please use the final published version (if applicable).

5 The effect of H^- continuum on Lava Planet Emission Spectra

Work in preparation **C.P.A. van Buchem**, M. Zilinskas, L. J. Janssen, Y. Miguel, and W. van Westrenen

Abstract

Hot rocky exoplanets (HREs) have the potential to reveal their interior makeup through studies of their atmospheric compositions thanks to surface lava oceans creating a direct interface between their interior and exterior reservoirs. Recent observations and modelling efforts point suggest that HREs may be able to support volatile bearing atmospheres. The extent to which volatile species can overwhelm lava composition specific signals in atmospheric spectra in such systems is as of yet not fully understood.

We aim to model volatile bearing HRE atmospheres and to understand how the presence of volatiles affects thermal emission spectra of these planets. The presence of free-electrons, due to the abundance of vaporised and subsequently ionized (alkali) metals, in a hot hydrogen-bearing atmosphere, suggests that H^- continuum opacity likely plays an important role in HRE atmospheres. It is already well established that the H^- continuum is highly influential in the atmospheres of stars and hot gas-giants, in this work we asses its impact on the atmospheres of HREs.

We make use of a self-consistent 1D forward model to estimate atmospheric chemical abundances, temperature-pressure structures, and thermal emission spectra, including feedback from the molten surface on the atmosphere.

We find that HREs with surface temperatures $\gtrsim$2500 K, even at a hydrogen volume mixing ratio of 10^{-5} in a 0.1 bar atmosphere, can lead to H^- continuum opacity dominating the features of the emission spectrum. As a result, spectral features of abundant atmospheric species (e.g. H_2O and SiO) are suppressed, and the planet's overall emission increases. This occurs because H^- opacity raises the photosphere to higher altitudes (with respect to atmospheres without H^- continuum absorption), where the temperature is higher in thermally inverted HRE atmospheres.

A strong H^- continuum could make it difficult to characterize the atmospheric composition of HREs due to the lack of/weakened strength of specific spectral features. However, due to the fact that abundant free-electrons are required for strong H^- opacity and that their main source is from ionized metals, the detection of a strong H^- continuum could be a potential indication of the presence of a surface lava ocean.

5.1 Introduction

Observations of hot rocky exoplanets (HREs) may have the potential to enable the inference of their interior compositions based on their atmospheric composition. Due to their short orbits, these planets have surface temperatures that can reach well above the eutectic melting point of silicate rocks ($\gtrsim$ 1500 K) making the existence of surface lava oceans very likely. Lava oceans could act as direct interfaces between the interiors and atmospheres of these planets (Léger et al. 2009; Henning et al. 2018; Boukaré et al. 2022). Understanding how the composition of a surface lava ocean influences the atmospheric composition of an HRE under varying temperatures, pressures, and volatile abundances, and quantifying the effect that this has on emission spectra is key to unlocking these windows into rocky planet interiors.

The modelling of lava oceans on HREs has historically been done under the simplifying assumption that no volatile elements (such as H, C, N, S, and P) are present in either the atmosphere or the interior of these planets (Schaefer & Fegley Jr. 2004; Miguel et al. 2011; Ito et al. 2015; Kite et al. 2016; Nguyen et al. 2020; Zilinskas et al. 2022; van Buchem et al. 2023; Wolf et al. 2023; Seidler et al. 2024). In recent years, an increasing number of both theoretical and observational studies have shown that it is plausible for HREs to contain volatile species. For example, magma oceans may potentially harbour large reservoirs of water (Hirschmann 2012; Lebrun et al. 2013; Dorn & Lichtenberg 2021; Kite & Schaefer 2021) and JWST observations of 55-Cnc e hint at the possible presence of a significant volatile atmosphere (Hu et al. 2024).

As such, the forward modelling of HRE atmospheres and their emission spectra has started to include volatile elements (Miguel 2018; Zilinskas et al. 2020, 2021). Piette et al. (2023) and Zilinskas et al. (2023) have shown that atmospheres that are a combination of vapor from a 'dry' (volatile-free) lava ocean and volatile atmospheric species (e.g. H_2O, CO, CO_2) may provide limited opportunities for observing lava ocean signatures in the infrared. Charnoz et al. (2023) and van Buchem et al. (2024) have shown that including volatile species in the lava ocean vaporisation reactions can lead to an increase in the abundance of all vapour elements. Falco et al. (2024) have studied the effect of lava vaporisation into an H atmosphere on emission spectra of HREs, finding that the existence of a thermal inversion may not a-priori exclude the presence of H in the atmosphere. In this work, we make use of LavAtmos 2.0 (van Buchem et al. 2024), which is able to take into account the effect of volatile elements (C, H, N, S, and P) to specifically investigate the effect of the HH^- continuum on HRE spectra.

The H^- continuum was first discovered to be of importance in the context of stellar atmospheres (e.g. Wildt 1939; Chandrasekhar 1945; John 1989) and has also been shown to be an important source of opacity in hot-Jupiters (Arcangeli et al. 2018; Lothringer et al. 2018; Parmentier et al. 2018). For H^- absorption to take place, the presence of both H and free-electrons is required. In previous

work where volatile-free atmospheres were assumed (Schaefer & Fegley 2009; Miguel et al. 2011; Kite et al. 2016; Zilinskas et al. 2022), no H was present, and in colder rocky-planet atmospheres containing volatiles, the concentration of free-electrons is not significant enough. HREs, however, have now been shown to potentially contain both H in their atmospheres and an abundance of free-electrons thanks to the presence of (alkali) metals vaporising from their surface lava oceans at high temperatures. Hence, H^- continuum absorption may potentially be of great importance to obtain a proper interpretation of HRE atmospheric emission spectra.

In this work, we use a self-consistent 1D modelling framework to show that even at low abundances H in HRE atmospheres can lead to significant H^- absorption across a range of equilibrium temperatures. We investigate the range of parameters within which this is the case and assess the effects this could have on the interpretation of HRE emission spectra.

5.2 Methods

5.2.1 Forward model

The forward model we use for this work is similar to that used in Zilinskas et al. (2022) and Zilinskas et al. (2023), but has been updated with the most recent versions of the component codes, as described in Zilinskas et al. (in rev) and Van Buchem et al. (in rev).

The model starts with calculating the melt-vapour composition for given melt-oxide (SiO_2, MgO, Al_2O_3, TiO_2, FeO, CaO, Na_2O, and K_2O) weight percentages and total atmospheric volatile element abundances (H, C, N, S, and P) . This is done using LavAtmos 2 (van Buchem et al. 2024), a vaporisation code that allows for volatile element abundances to be included in vaporisation calculations self-consistently. LavAtmos 2 makes use of the geothermodynamic code MELTS (Ghiorso & Sack 1995; Asimow & Ghiorso 1998; Ghiorso et al. 2002; Gualda et al. 2012; Ghiorso & Gualda 2015) to calculate the activities of melt species. The chemical-equilibrium constants used in the vaporisation reactions were calculated using data from the JANAF-NIST database (Chase 1998). In this study we assume the composition of the melts is equal to the composition of the Bulk Silicate Earth (BSE) (Palme & O'Neill 2003). We tested a range of different atmospheric volatile element abundances, each representing end-member compositions observed in our Solar System (see Table **??**).

The output from the vaporisation code is passed on to the atmospheric thermochemical equilibrium code FastChem 3 (Stock et al. 2018, 2022; Kitzmann et al. 2024) to calculate chemical compositions across a wide temperature-pressure (TP) grid. These abundances are then used by HELIOS (Malik et al. 2017, 2019; Whittaker et al. 2022) to calculate a TP profile. If the temperature at the bottom of the atmosphere, as determined by the TP profile, does not

coincide with the initial guess of the surface temperature, the code reiterates using the the temperature at the bottom of the TP profile as a new starting point. This is repeated until the difference between the initial temperature used for the vaporisation calculations differs by less than 25 K with the surface temperature derived from the TP profile.

The heat redistribution is parametrised using an f-factor (Hansen 2008) approximation based on the longwave optical depth of the atmosphere (Koll 2022) as included in HELIOS. We used a standard diatomic adiabatic coefficient $\kappa = 2/7$ for convective adjustment.

Once the model converges on a surface temperature, FastChem 3 is used again to calculate the chemical abundances along the finalized TP profile. The final temperature and chemical structure of the atmosphere are passed on to petitRADTRANS (Mollière et al. 2019, 2020) which produces an emission spectrum between 0.3 and 28 μm.

The opacities used in this work, in both HELIOS and petitRADRANS, are the same as those used for Zilinskas et al. (in rev.). A complete list is given in the appendix (Table 5.2)[1]. These opacities were either taken from the DACE[2] database or calculated using HELIOS-K (Grimm & Heng 2015; Grimm et al. 2021). Due to the H^- opacity being the focus of this paper, we discuss it in detail in the following subsection.

We used star-planet system parameters resembling those of 55-Cnc e as an illustrative example to demonstrate the overall influence of H^- on HRE atmospheres. This work does not aim to explain 55-Cnc e specifically. We use a planet radius of 1.946 $R_\oplus$, a planet surface gravity of 2222 cm s^{-2}, a stellar radius of 0.98 $R_\odot$, a stellar temperature of 5214 K, and a metallicity of 0.35. For the spectrum of the star we use the same spectrum that was used for 55-Cnc in Hu et al. (2024). This spectrum combines the near-infrared and infrared spectra of 55-Cnc as gathered during the observations presented in Hu et al. (2024) along with an interpolation of a `PHOENIX` model (Husser et al. 2013), and the spectrum from Crossfield (2012) for the shorter wavelengths.

5.2.2 H^- opacity

H^- has been known as the dominant source of continuum opacity in stellar atmospheres since first pointed out by Wildt (1939). The two mechanisms through which H^- absorbs are bound-free (*bf*) absorption and free-free (*ff*) absorption.

Bound-free absorption (also known as photo-detachment) takes place when a photon collides with an H^- ion and the photon carries enough energy to free the extra electron from the H^- ion, producing a free electron and a neutral H

[1] ExoMol (`https://www.exomol.com/`) was used as the main source for line list recommendations.

[2] https://dace.unige.ch/

Table 5.1: Volatile element compositions in mole fractions of the total volatile pressure in the atmosphere

	H	C	N	S	P
Solar	9.996E-01	2.691E-04	6.758E-05	1.318E-05	2.569E-07
Earth	5.126E-03	2.600E-04	9.946E-01	0.000E+00	0.000E+00
Titan	2.824E-02	6.627E-03	9.334E-01	0.000E+00	0.000E+00
Venus	3.900E-05	9.320E-01	6.784E-02	1.470E-04	0.000E+00

Notes. These composition are not including the species vaporised from the lava ocean. Solar composition was derived from Asplund et al. (2009). The Earth, Titan, and Venus atmospheric compositions were taken from Morley et al. (2017).

atom:

$$H^- + \gamma \rightarrow H + e^- \tag{5.1}$$

Where γ is a photon and e^- a free electron. The binding energy of an electron with an H atom is 0.7542 eV (Frolov 2015) and as such, this absorption method only impacts photons with a wavelength ≤ 1.644 μm.

Free-free absorption occurs when a photon is absorbed by an electron accelerating in the field of a neutral hydrogen atom (John 1991), as given in the reaction:

$$H + e^- + \gamma \rightarrow H + e^- \tag{5.2}$$

This type of absorption can take place at any given photon energy and is therefore not limited to specific wavelengths. However, its opacity does increase with wavelength and becomes significant (for this work) from the near infrared onwards. Unlike *bf* absorption, which is dependent on H^- abundance, *ff* absorption is dependent on the abundance of neutral H and free-electrons (e-).

The different regimes in which these types of absorption are dominant are shown in Figure 5.1. The models used in this figure are those of John (1988), and are also used in the radiative transfer codes to calculate the planetary emission spectra (HELIOS and petitRADTRANS, see Section **??**). These models are in good agreement with other commonly used parametrisations provided by Gray (2022) based on data gathered by Wishart (1979) and Bell & Berrington (1987) for *bf* and *ff* absorption respectively.

5.3 Results

The emission spectra of HREs can change significantly depending on their atmospheric composition. This is illustrated in Figure 5.2, where we compare the emission spectra (panel *a*) and TP profiles (panel *b*) of three atmosphere types. In blue, we show a pure (no lava vapour) 0.1 bar volatile atmosphere of

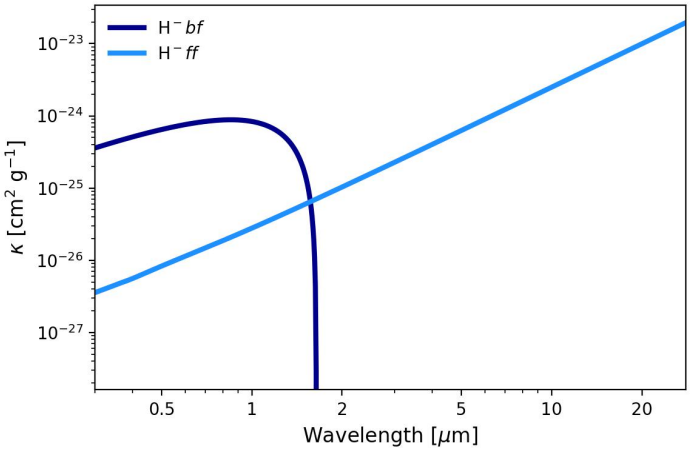

Figure 5.1: H- *bf* and *ff* opacities: Plotted using the models from John (1988) at 3000 K, 1e-4 bar, and assuming H-, H, and e- volume mixing ratios (VMRs) of ≃ 2.21e-8, 4.48e-1, and 5.79e-2 respectively. These values are representative for what we find in a 0.1 bar atmosphere, at 0.016 AU, for a BSE composition melt (see section **??**).

solar-like composition (see Table 5.1)[3], in red a pure lava vapour atmosphere (no volatiles), and in orange a 'hybrid' atmosphere containing both 0.1 bar of volatile elements and lava vapour. All other system parameters used for these models are the same (as specified in section 5.2).

The volatile-only atmosphere has a non-inverted TP profile and has a spectrum dominated by H_2O absorption features in the near- and far-infrared. This is in contrast with the vapour only atmosphere, which has a fully inverted TP profile. This is due to the presence of strong optical absorbers, such as TiO, causing the atmosphere to be more opaque in the optical than in the infrared (Gandhi & Madhusudhan 2019), and is a common feature of HRE atmospheres (Zilinskas et al. 2022; Seidler et al. 2024). The vapour only spectrum also has clear spectral features of atomic Na and K in the optical and SiO in the infrared (around 9 μm). The 'hybrid' atmosphere, containing both volatile species and lava vapour, contrasts starkly with the other two. Emission is greater, and the emission spectrum is dominated by a continuum, lacking strong features of atmospheric species. The TP profile of this atmosphere bears some resemblance to the lava-vapour case, except with a non-inverted almost isothermal lower atmosphere (pressures above 1e-3 bar). To understand why the emission spectrum from the hybrid atmosphere looks so different, we have to look at its chemical structure and contribution to the opacity throughout the atmosphere.

[3]Due to the absence of a lava ocean determining the O abundance of the atmosphere, we used a solar O abundance.

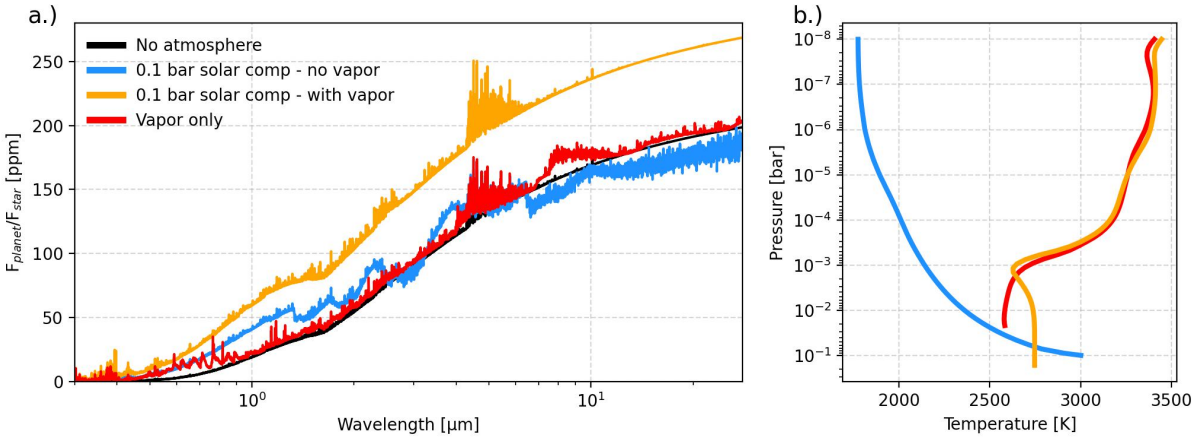

Figure 5.2: Comparing atmosphere types: Emission spectra (panel *a*) and TP profiles (panel *b*) of three different atmosphere types. A pure volatile atmosphere (of solar-like composition) is shown in blue, a pure volatile free (BSE) lava vapour atmosphere is shown in red, and the combination of a volatile with lava vapour atmosphere is shown in orange. As a point of reference we also plot the emission spectrum in the case of no atmosphere being present in black.

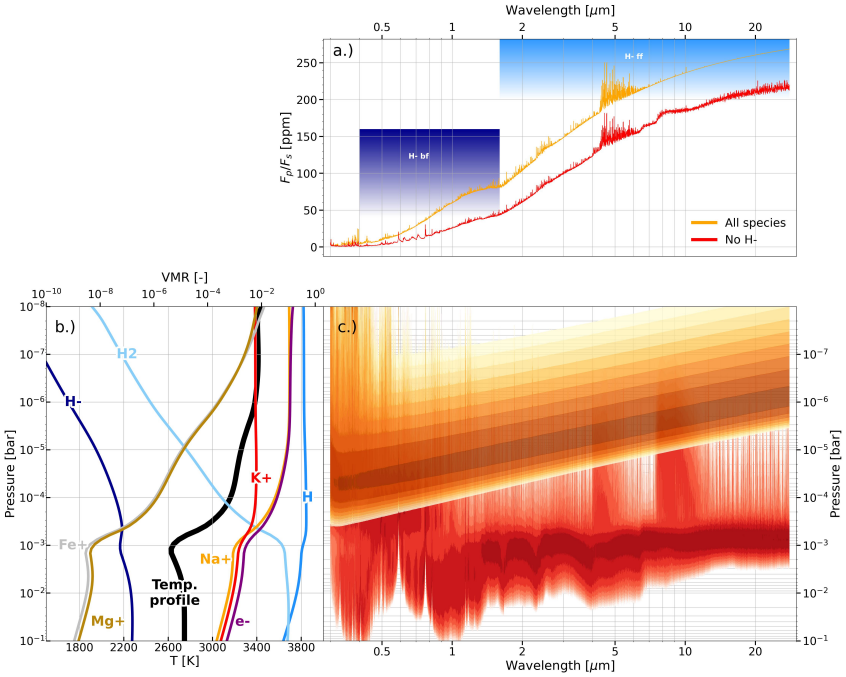

Figure 5.3: Overview of an atmosphere containing both lava vapor and volatile elements: The top panel (a) shows the spectrum of an HRE when including H^- continuum opacity in orange and the spectrum of the same atmosphere when H^- continuum opacity is ignored. The regions in which H^- bf and ff absorption dominate are indicated in dark blue and light blue respectively. The bottom left panel (b) shows the VMR of relevant species in the atmosphere, along with the TP profile. In the bottom right panel (c), the opacity contribution as a function of wavelength and pressure is shown for when H^- continuum opacity is (in orange) and is not (in red) included.

Figure 5.3 provides an overview of a number of properties of the 'hybrid' atmosphere. In the top panel (panel *a*), the full emission spectrum of the 'hybrid' atmosphere (shown in orange) is compared to the emission spectrum of the same atmosphere excluding H^- continuum opacities (shown in red). When H^- is excluded from the radiative transfer model used to produce the emission spectrum (see section 5.2.1), the resulting spectrum looks more similar to the vapor only model at a lower brightness, with K and Na lines visible in the optical and the SiO feature visible around 9 μm. The bottom right panel (panel *c*) explains the source of these differences. For the two spectra, the normalized opacity contribution is shown in the respective colors. When including the H^- continuum opacity the photosphere is located higher up in the atmosphere, from 1e-4 bar in the optical to 1d-6 bar in the infrared. When the H^- continuum opacity is excluded, the photosphere is located just below 1e-4 bar in the optical and around 1e-3 bar in the infrared. Due to the temperature-pressure profile being inverted (see panel *b* in the bottom left), the photosphere of the spectrum that includes H^- continuum opacity is emitting radiating from a region with a much higher temperature (around 3300 K) than the case without H^- continuum opacity (around 2600 K). As a result, the temperature brightness of the 'hybrid' spectrum is much higher than that of the other two models seen in Figure 5.2. We also see in this example how the H^- continuum opacity dominance does not allow for other spectral features to contribute significantly to the emission spectrum of the atmosphere.

Panel *b* includes the volume mixing ratio (VMR) of a number of relevant species. As discussed in section 5.2.2, H^- bf absorption is dependent on the abundance of H-, while H^- ff absorption is linked to the abundance of H and free electrons (e-). While H_2 dominates over H at the surface, as pressure decreases and (below 1e-3 bar) temperature increases, H_2 dissociates to form H. The abundance of e- is dependent on the abundance of ionized metals from which the e- have escaped through thermal dissociation. This is reflected in the strong correlation between the e- abundance and the abundance of the four major metal ions Na+, K+, Mg+, and Fe+. Below 1e-3 bar, K+ is the main source of free electrons with Na taking over beyond 1e-3 where the thermal inversion starts. From 1e-7 bar onward, Fe+ and Mg+ also start to contribute significantly to the e- abundance. The start of the photosphere of the 'hybrid' model at around 1e-5 bar, coincides with the e- abundance reaching a VMR of around 1e-1.

For H^-, its abundance follows the general trend of the TP profile at higher pressures and lower temperatures (in the case of this particular atmosphere), increasing with higher temperatures thanks to an increase in H and e-. However, as the temperature reaches beyond about 2800 K, the H^- abundance starts to decrease with increasing temperature. This is due to the thermal dissociation of H^- into H and e- (similarly to the formation of the positive metal ions).

In the following subsections we investigate the effects of varying atmospheric

H abundance, temperature, and volatile composition on the H^- continuum opacity.

5.3.1 Adding H to a lava planet atmosphere

To understand how much hydrogen must be present in the atmosphere for H^- continuum absorption to have a significant impact on the emission spectrum, we calculated the emission spectra of an HRE with a volatile atmosphere of varying total pressures (from 1e-8 up to 1e-1 bar) containing only H as volatile element. The results can be seen in Figure 5.4.

In panel *a* of Figure 5.4, the emission spectrum of the test planet in the case without an atmosphere is shown in black. The emission spectrum produced when including a pure lava vapour atmosphere is shown in yellow. Comparing with the no atmosphere case, we see that including a lava vapour atmosphere leads to the presence of emission features of K and Na in the optical and of SiO and SiO_2 in the infrared (around 9 μm). From this point onward, emission spectra are calculated for atmospheres containing an increasing amount of H in the atmosphere.

Adding just 1e-8 bar of total H pressure already leads to a shift in the spectrum, with a slight increase in emission at wavelengths beyond μm. With each increasing order of magnitude of added total elemental H abundance to the atmosphere, we see an increase in emission. This effect becomes more substantial towards longer wavelengths. At 1e-5 bar total H pressure the SiO and SiO_2 features around 9 μm are no longer discernible in the spectrum. At this H abundance, a significant increase in optical emission also starts taking place, which starts obscuring the alkali features. From 1e-4 bar total H pressure and upwards, the calculated emission spectra are entirely dominated by the H^- continuum. Increasing the total H abundance leads to a higher brightness temperature but no significant changes in the spectral features.

In panel *b* of Figure 5.4 the corresponding TP profiles of each of the models (except the no atmosphere case) are shown. The vapour only and low H abundance models all have very similar TP profiles and are superimposed on each other. From 1e-4 bar added H we start seeing a divergence in the lower atmosphere to higher pressures and higher temperatures. From 1e-3 bar onwards, moving up in the atmosphere to lower pressures, all TP profiles follow the same general trend. As we have seen in Figure 5.3, even when no H^- continuum opacity is included, the photosphere is located at around 1e-3 bar at its lowest point. As a result, the differences in TP structure that we are seeing deeper in the atmosphere do not affect the emission spectra. Hence, the differences that we are seeing in the spectra in panel *a* are due to the photosphere rising up to lower pressures and, due to the temperature inversion, higher temperatures leading to an increase in emission.

These models make it clear that only a small amount of H is required for H^- continuum opacity to affect the emission spectrum of HREs. In Figure 5.5

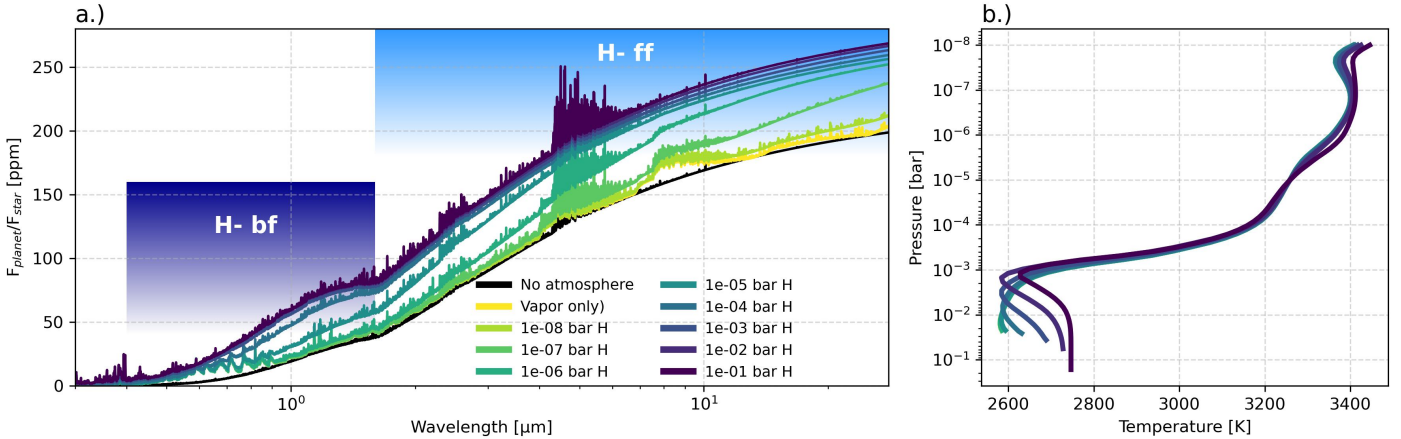

Figure 5.4: Adding H to a lava ocean atmosphere: The thermal emission spectra of our test planet plotted at varying total atmospheric H pressures are plotted in panel *a*. Note that this refers to the total H abundance. Panel *b* shows the corresponding TP profiles.

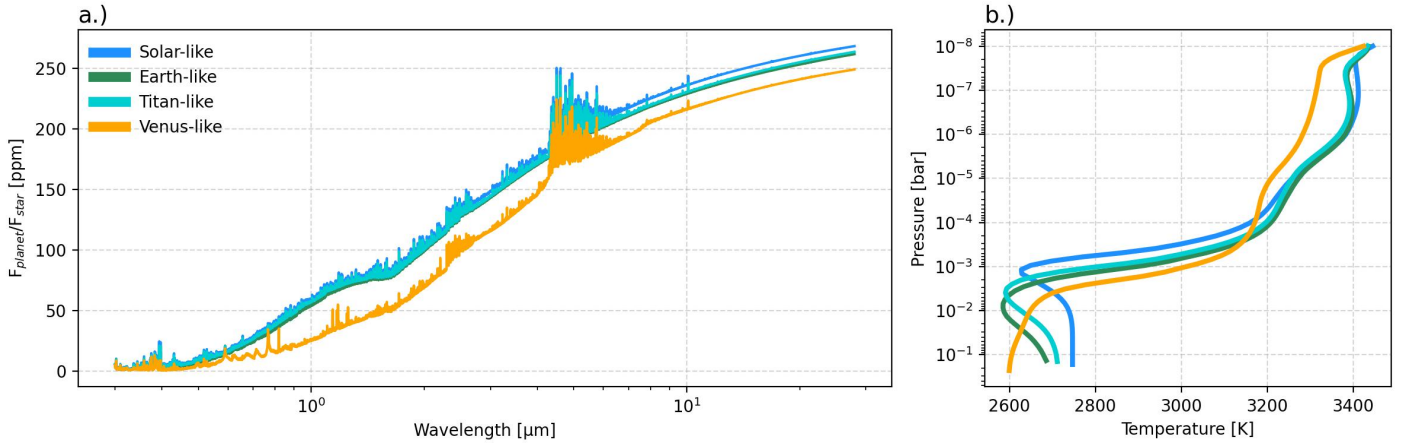

Figure 5.5: Emission spectra of complex volatile atmospheres: For each model a 0.1 bar of volatiles was assumed. The volatile compositions of each are given in Table 5.1.

we show that this is also the case for 'complex' volatile atmospheres, containing H, C, N, S, and P. In panel *a* the emission spectra of atmospheres with 0.1 bar volatiles are shown. Volatile abundances are based on a solar-like composition (Asplund et al. 2009), and Earth-like, Titan-like, and Venus-like compositions (Morley et al. 2017) (see Table 5.1). The corresponding TP profiles are shown in panel **b**.

The Solar-like, Earth-like, and Titan-like atmospheres (with H mole fractions of 9.996e-1, 5.126e-3, and 2.824e-2 respectively) are all significantly affected by the H^- minus continuum opacity - consistent with what we see in the pure H atmospheres in Figure 5.4. The Venus-like atmosphere has the least amount of H (mole fraction of 3.9e-5) and is therefore least affected by the H^- continuum opacity, but even so we see (most clearly in the far infrared beyond around 8 μm) that the spectrum is affected by the H^- ff opacity similarly to the 1e-6 bar pure H atmosphere in Figure 5.4 (which has a similar total H abundance).

From these models it is clear that an HRE requires very little H in its atmosphere for the emission spectrum to be dominated by H absorption. With as little as 1e-6 bar total H pressure obscuring vaporised lava features and 1e-4 bar total H being enough for the H^- continuum opacity to dominate the entire spectrum. However, as seen in Figure 5.2, more than just H is required in the atmosphere for H^- continuum opacity to affect the emission spectrum.

5.3.2 Sensitivity to temperature

As explained in section 5.2.2, free electrons are needed for atmospheric H^- continuum absorption to take place. They are necessary for H-*bf* absorption to form H^- ions and they are necessary for the H-*ff* absorption reaction to be able to take place (see equation 5.2). The main source of free electrons in HRE atmospheres is from (alkali) metals which enter the atmosphere through vaporisation from lava and are subsequently ionised at high temperatures. The most important of these ions for a melt of BSE composition (Palme & O'Neill 2003) are Na^+, K^+, Fe^+, and Mg^+. The (surface) temperature of the HRE dictates the amount and composition of vapour entering the atmosphere (van Buchem et al. 2023, 2024) and is a measure of the extent of thermal ionization taking place.

Furthermore, H-*bf* requires H atoms for H^- to be able to form and H-*ff* requires H atoms for the absorption reaction to take place. The formation of H over H_2 in an atmosphere is both pressure and temperature dependent, with higher temperatures favouring the formation of H. This adds another temperature dependence to the strength of H^- continuum opacity.

To assess how these temperature dependences affect the abundance of the relevant atmospheric species, the TP structure, and the resulting emission spectrum, we lowered the temperature of the test planet by varying the orbital distance from its host star from 0.016 AU to 0.032 AU. In Figure 5.6 we show how

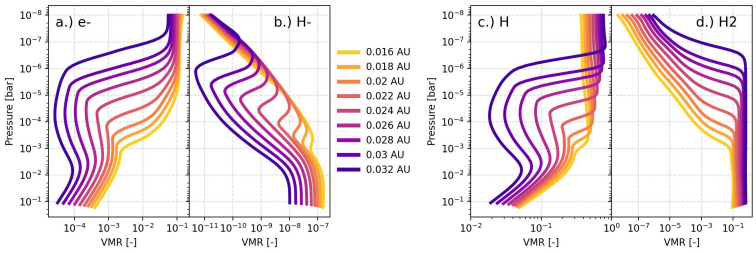

Figure 5.6: Abundance of atmospheric species at varying orbital distances: Shown for atmosphere with solar relative volatile abundances at a total volatile pressure of 0.1 bar and a BSE lava composition.

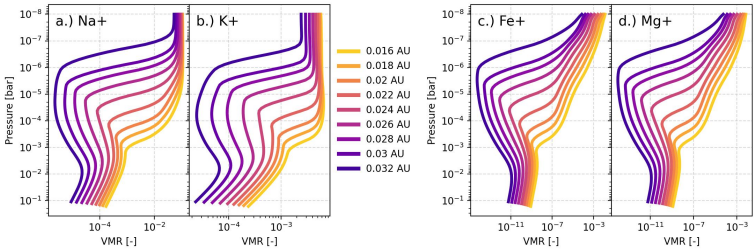

Figure 5.7: Abundances of metal ions at varying orbital distances: Shown for atmosphere with solar relative volatile abundances at a total volatile pressure of 0.1 bar and a BSE lava composition.

changing the orbital distance affects e-, H-, H, and H_2 abundances throughout the tested atmospheres. Figure 5.7 shows the same but for the key metal ion species (Na+, Mg+, Fe+, and Mg+). In Figure 5.8 we show the emission spectra and the TP profiles of these same models.

Comparing the e- abundances in panel *a* in Figure 5.6 and the metal ion abundances in Figure 5.7 with the TP profiles in panel *b* in Figure 5.8 clearly shows the positive relationship between temperature and atmospheric abundance of these species. In panels *c* and *d* the increase in H with temperature due to the dissociation of H_2 is illustrated.

Looking at panel *b* in Figure 5.6, we see that the H^- abundance has a positive relationship with temperature below about 2600 K. However, as temperatures reach beyond this point, the increase in thermal energy leads to the release of the captured electron, and H^- reverts to neutral H and a free electron. This explains the decrease in H^- abundance higher up in the atmospheres, even though we see an overall increase lower in the atmospheres where the temperatures are cooler.

The temperature dependences of the abundances of all the species required

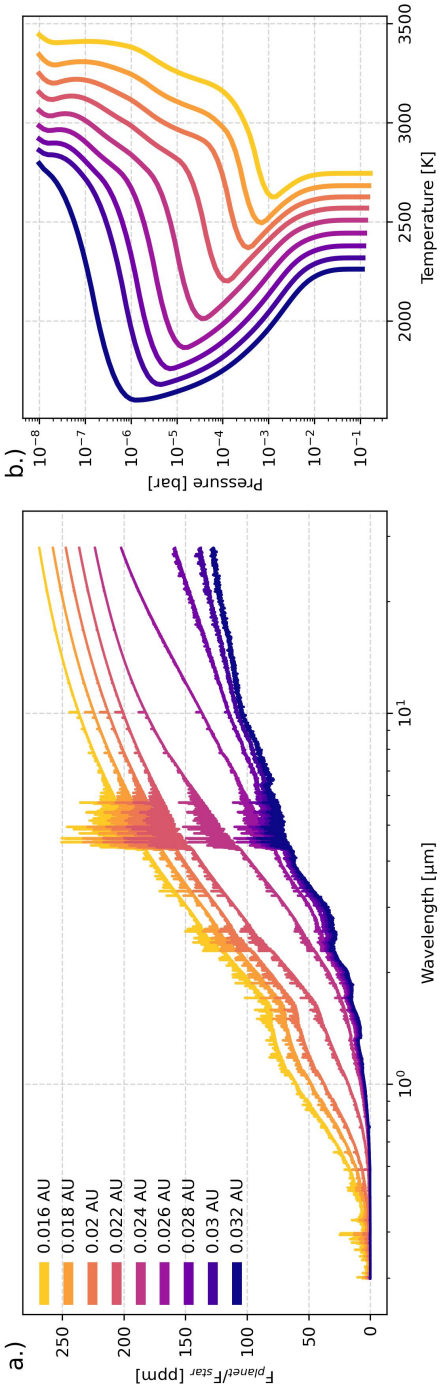

Figure 5.8: Emission spectra at varying orbital distances: Shown for atmospheres with solar relative volatile abundances at a total volatile pressure of 0.1 bar and a BSE lava composition.

for H^- continuum absorption causes emission spectra to vary strongly with temperature as well. Looking at panel *a* of Figure 5.8, we see that when the test planet is placed at a distance of 0.032 AU, surface temperature drops by 500 K, and at higher altitudes the drop is even greater (up to 1000 K with respect to the test planet at 0.016 AU). As a result the emission spectrum is far less bright, and it contains some visible spectral features. The drop in brightness of the emission spectrum is due to a combination of the photosphere being located at lower (and colder) altitudes due to a lack of H^- continuum opacity and a colder atmosphere overall. Without the H^- continuum dominating over other spectral features and colder atmospheric temperatures, we see some H_2O features in the optical wavelengths. There is also a hint of the SiO feature around 9 μm.

As the test planet orbital distance is lowered from 0.032 AU, our calculations indicate that at 0.026 AU (surface temperature of $\simeq$2400 K) there is a significant increase in emission in the infrared, obscuring any potential SiO features from a surface lava ocean. At 0.022 AU (surface temperature of $\simeq$2600 K) the H^- continuum also dominates over the optical lava ocean features - no spectral features are discernible anymore. Based on these models, which assume the presence of 0.1 bar of volatiles combined with vapour from a surface lava ocean, it appears that a rough temperature threshold from which point onwards the H^- continuum dominates the spectrum is when the majority of the atmosphere has a temperature greater than 2500 K.

5.4 Discussion

The dominance of the H^- continuum in HRE spectra at temperatures above approximately 2500 K in atmospheres containing hydrogen is such that it cannot be ignored when interpreting the spectra of these atmospheres.

The most significant change that we see in the emission spectra when including the H^- continuum is the large increase in flux emitted from the planet due to the photosphere moving up to higher altitudes and temperatures (see Figure 5.3). This can lead to a degeneracy in determining the surface temperature.

A potential way to overcome this degeneracy is by identifying distinct spectral features. As shown in Figure 5.2, both a vapour only and volatile only atmosphere have clear spectral features of the dominant species in their respective atmospheres. In an atmosphere dominated by the H^- continuum, none of these features are visible. The absence of spectral features in an H^- dominated spectrum will likely make it difficult to characterize the composition of these HREs.

However, as we have seen in sections 5.3.1 and 5.3.2, the opacity of the H^- continuum is heavily reliant on the presence of both H and free electrons in the atmosphere. Hence, if an emission spectrum is found to be dominated by the H^- continuum, this could be used in retrievals to place constraints on the H abundance of the atmosphere, and on the abundance of metal ions necessary

to produce the free-electrons. This has been shown to be of importance in studies on hot Jupiters, where including the H^- continuum in atmospheric retrievals has led to tighter constraints on the metallicity of the atmospheres of these planets (Arcangeli et al. 2018; Lothringer et al. 2018; Parmentier et al. 2018). In contrast with hot Jupiters, where metals may reach high up in the atmosphere through mixing with the interior, the dominant mechanism for metals to enter the atmosphere of an HRE would be through vaporisation of a surface lava ocean. Hence, strong H^- continuum emission could point to the presence of a surface lava ocean on an HRE.

5.5 Conclusion

We find that the H^- continuum from H-*bf* and H-*ff* absorption can dominate the emission spectrum of HREs. Even trace amounts of hydrogen in the atmosphere (as little as 10^{-6} total H partial pressure) can obscure the spectral features of other major atmospheric species. This also holds for planets with volatile but non-hydrogen dominated atmospheres - similar in composition to those of Earth, Titan, or Venus - may still experience significant effects from the H^- continuum in their emission spectra.

The presence of the H^- continuum leads to the photosphere of an HRE to move to higher altitudes than when no H^- continuum is included. As the atmospheres of HREs are generally inverted, this means that the photosphere is radiating from a region with a much greater temperature (around 500 K more) leading to a far brighter emission spectrum.

Due to the dependences of atmospheric H and free electron abundance on temperature, the impact of the H^- continuum is also heavily dependent on temperature. If the majority of an atmosphere has a temperature above approximately 2500 K, then we find that all other features are obstructed by the H^- continuum.

Due to the necessity of abundant free electrons in the atmosphere for H^- absorption to take place and the main source of free-electrons being ionized metals, finding a strong influence of the H^- continuum in an HRE atmosphere could be an indication of the existence of a surface lava ocean.

Acknowledgements

This work was supported financially through a Dutch Research Council (NWO) Planetary and Exoplanetary Science (PEPSci) grant awarded to Y.M. and W. van W.

Y.M and M.Z. acknowledge funding from the European Research Council (ERC) under the European Union's Horizon 2020 research and innovation programme (grant agreement no. 101088557, N-GINE). Part of this research was carried out at the Jet Propulsion Laboratory, California Institute of Technology, under a contract with the National Aeronautics and Space Administration.

Appendix

5.A Opacities

Table 5.2: List of opacities and their sources used to calculate the temperature-pressure profiles and emission spectra in this work. Those with DACE as indicated source were taken directly from the DACE database (`https://dace.unige.ch/`). For the other species, the opacities were calculated using HELIOS-K (`https://github.com/exoclime/HELIOS-K`) (Grimm & Heng 2015; Grimm et al. 2021).

Species	Source	Line list	Line list reference
Al	DACE	VALD	Ryabchikova et al. (2015)
AlH	HELIOS-K	AlHambra	Yurchenko et al. (2018c)
AlO	HELIOS-K	ATP	Patrascu et al. (2015)
C	DACE	Kurucz	Kurucz (1992)
C_2	DACE	8states	Yurchenko et al. (2018b)
C_2H_2	DACE	aCeTY	Chubb et al. (2020)
C_2H_4	DACE	MaYTY	Mant et al. (2018)
Ca	DACE	VALD	Ryabchikova et al. (2015)
CaH	HELIOS-K	MoLLIST	Li et al. (2012); Bernath (2020)
CaO	HELIOS-K	VBATHY	Yurchenko et al. (2016)
CaOH	DACE	OYT6	Owens et al. (2022)
CH	DACE	MoLLIST	Masseron et al. (2014); Bernath (2020)
CH_3	DACE	AYYJ	Adam et al. (2019)
CH_4	DACE	YT34to10	Yurchenko et al. (2017)
CN	HELIOS-K	Trihybrid	Syme & McKemmish (2021)
CO	DACE	Li2015	Li et al. (2015)
CO_2	DACE	HITEMP & UCL-4000[c]	Rothman et al. (2010); Yurchenko et al. (2020)
CS	DACE	JnK	Paulose et al. (2015)
Fe	DACE	VALD	Ryabchikova et al. (2015)
FeH	DACE	MoLLIST	Dulick et al. (2003)
H_2^+	DACE	ADJSAAM	Amaral et al. (2019)
H_2CO	DACE	AYTY	Al-Refaie et al. (2015)
H_2O	DACE	POKAZATEL	Polyansky et al. (2018)
H_2O_2	DACE	APTY	Al-Refaie et al. (2016)
H_2S	DACE	AYT2	Azzam et al. (2016)
H_3O^+	DACE	eXeL	Yurchenko et al. (2020)
HCN	HELIOS-K	Harris	Barber et al. (2014)
HNO_3	DACE	AIJS	Pavlyuchko et al. (2015)
HS	HELIOS-K	GYT	Gorman et al. (2019)
K	DACE	VALD	Ryabchikova et al. (2015)
KOH	DACE	OYT4	Owens et al. (2021)
Mg	DACE	Kurucz	Kurucz (1992)
MgH	HELIOS-K	MoLLIST	GharibNezhad et al. (2013); Bernath (2020)
MgO	HELIOS-K	LiTY	Li et al. (2019)
N	DACE	VALD	Ryabchikova et al. (2015)
N_2	DACE	WCCRMT	Western et al. (2018)
N_2O	DACE	HITEMP2019	Hargreaves et al. (2019)
Na	DACE	VALD	Ryabchikova et al. (2015)
NaH	HELIOS-K	Rivlin	Rivlin et al. (2015)
NaO	DACE	NaOUCMe	Mitev et al. (2022)
NaOH	DACE	OYT5	Owens et al. (2021)
NH	DACE	MoLLIST	Fernando et al. (2018)
NH_3	DACE	CoYuTe	Coles et al. (2019)
NO	DACE	XABC	Wong et al. (2017); Qu et al. (2021)
NO_2	DACE	HITEMP2019	Hargreaves et al. (2019)
NS	DACE	SNaSH	Yurchenko et al. (2018a)
OH	DACE	HITEMP	Rothman et al. (2010)
OH^+	DACE	MoLLIST	Hodges & Bernath (2017)

P	DACE	VALD	Ryabchikova et al. (2015)
PC	DACE	MoLLIST	Ram et al. (2014); Qin et al. (2021)
PH	HELIOS-K	LaTY	Langleben et al. (2019)
PH_3	DACE	SAlTY	Sousa-Silva et al. (2015)
PN	DACE	YYLT	Yorke et al. (2014)
PO	DACE	POPS	Prajapat et al. (2017)
PS	HELIOS-K	POPS	Prajapat et al. (2017)
S	DACE	VALD	Ryabchikova et al. (2015)
Si	DACE	VALD	Ryabchikova et al. (2015)
SiH	HELIOS-K	Slightly	Yurchenko et al. (2018c)
SiH_2	HELIOS-K	CATS	Clark et al. (2020)
SiH_4	DACE	OY2T	Owens et al. (2017)
SiN	DACE	SiNfull	Semenov et al. (2022)
SiO	HELIOS-K	SiOUVenIR	Yurchenko et al. (2022)
SiO_2	DACE	OYT3	Owens et al. (2020)
SiS	DACE	UCTY	Upadhyay et al. (2018)
SO	DACE	SOLIS	Brady et al. (2024)
SO_2	ExoMol	ExoAmes	Underwood et al. (2016a)
SO_3	ExoMol	UYT2	Underwood et al. (2016b)
Ti	DACE	VALD	Ryabchikova et al. (2015)
TiH	HELIOS-K	MoLLIST	Burrows et al. (2005); Bernath (2020)
TiO	HELIOS-K	Toto	McKemmish et al. (2019)

Scattering and continuum

CO, CO_2, H		Scattering	
H_2, N_2, O_2		Scattering	
H^-		Continuum (bf & ff)	John (1988)
H_2-H_2	petitRADTRANS	CIA	Borysow et al. (2001); Borysow (2002)
CO_2-CO_2	petitRADTRANS	CIA	Karman et al. (2019)
O_2-O_2	petitRADTRANS	CIA	Karman et al. (2019)
N_2-H_2	petitRADTRANS	CIA	Karman et al. (2019)
N_2-N_2	petitRADTRANS	CIA	Karman et al. (2019)